X-ray statistics

	M257Y/GαCT light activated[a]
Data collection	SLS, X06SA
Space group	H32
Cell dimensions	
a, *b*, *c* (Å)	242.2, 242.2, 109.8
α, β, γ (°)	90, 90, 120
Resolution (Å)	45-3.3 (3.48-3.3)[b]
R_{sym} or R_{merge}	0.18 (0.66)
$I/\sigma I$	8.5 (1.8)
Completeness (%)	94.8 (65.4)
Redundancy	5.7 (2.9)
Refinement	
Resolution (Å)	45-3.3
No. reflections	17649
R_{work}/ R_{free}	0.217/0.259
No. atoms	2781
M257Y/GαCT	2680
Ligand/ion	92
Water	9
B-factors	
Protein	75.1
Retinal	96.5
Water	70.8
R.m.s deviations	
Bond lengths (Å)	0.011
Bond angles (°)	1.40

[a] Merged data from three crystals
[b] Highest resolution shell is showed in parenthesis

Supplementary Table1: Data collection and refinement statistics

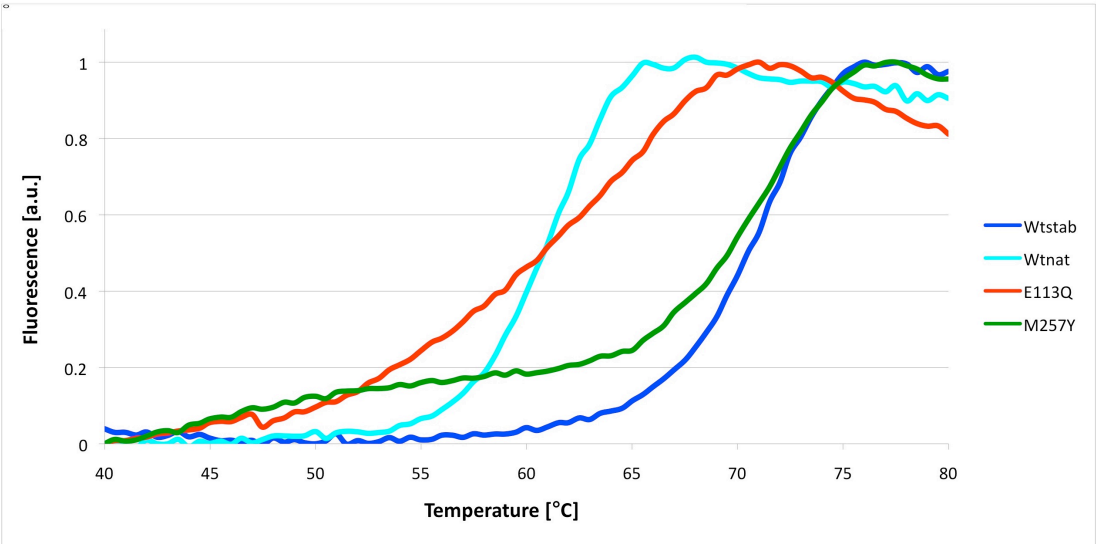

Supplementary Figure 1: Thermal shift denaturation assay of rhodopsin mutants. The stability of native wild-type rhodopsin (cyan) and stabilized N2C/D282C rhodopsin with (blue) and without the E113Q$^{3.28}$ (red) or M257Y$^{6.40}$ (green) mutations is compared using thermal denaturation in the presence of a thiol specific maleimide fluorochrome CPM (N-[4-(7-diethylamino-4-methyl-3-coumarinyl)phenyl]malemeide) as described(1). Introduction of the stabilizing disulfide increases thermal stability of opsin by about 10°C compared to the wild type isolated from bovine retina. Neutralization of the Schiff base counterion by the E113Q$^{3.28}$ mutation is strongly destabilizing while the M257Y$^{6.40}$ mutant is not.

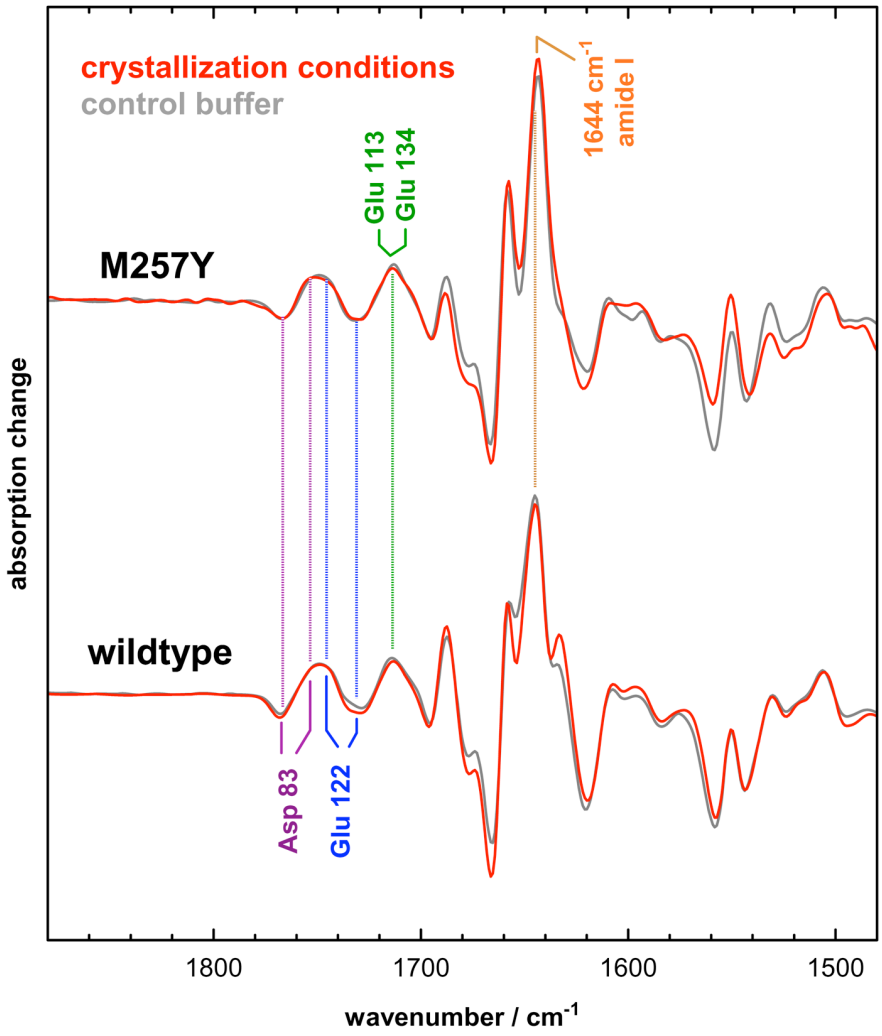

Supplementary Figure 2: Rhodopsin adopts metarhodopsin-II under crystallization conditions. Light-induced FTIR difference spectra *photoproduct minus dark state* of the M257Y$^{6.40}$ mutant and of wild type rhodopsin (both with the stabilizing N2C/D282C mutation) were recorded at 4°C under crystallization and control conditions. Under both conditions, wildtype and the M257Y$^{6.40}$ mutant receptors adopt their active metarhodopsin-II conformation upon photoactivation, as evident from the spectral patterns due to D83$^{2.50}$ and E122$^{3.37}$ and the protonation signatures of E134$^{3.49}$ and E113$^{3.28}$. Despite smaller alterations in the range of the amide I difference bands around 1650 cm^{-1}, the meta-II marker band at 1644 cm^{-1} is observed to full extent under both conditions. FTIR difference spectroscopy was performed as described(2, 3) in a lipid/detergent mixture similar to the crystallization conditions supplemented with control (200 mM MES buffer and 200 mM NaCl at pH4.5) and crystallization buffer (3.2 M ammonium sulfate and 100 mM sodium acetate at pH 4.5 in the presence of a 10-fold excess of the GαCT peptide). We gratefully acknowledge Dr Reiner Vogel from the University of Freiburg for performing the FTIR experiments.

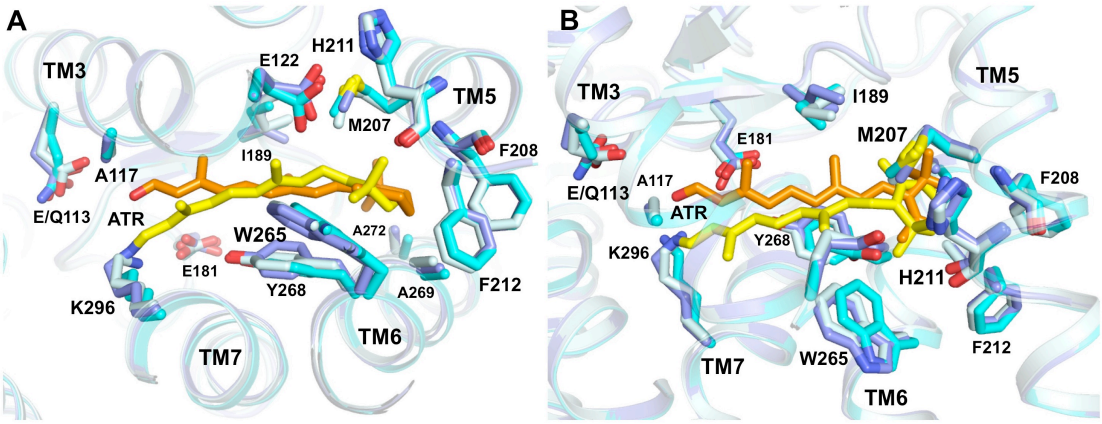

Supplementary Figure 3: Retinal binding site in several active states of rhodopsin

Superposition of retinal binding sites (A: extracellular view, B: membrane view) in opsin (grey) and the constitutively active mutants E113Q$^{3.28}$ (cyan) and M257Y$^{6.40}$ (blue). Retinal in both the E113Q$^{3.28}$ (orange) and M257Y$^{6.40}$ (yellow) is buried deep into the cleft between TM5 and TM6 with nearly identical positions of the β-ionone ring. Retinal in the M257Y$^{6.40}$ structure is however rotated along its axis with respect to the E113Q$^{3.28}$ active-state(4), batho(5), lumi(6) and ground-state rhodopsin(7). The polyene in the M257Y$^{6.40}$ structure furthermore points towards the covalent bond with K296$^{7.43}$ accompanied by a small rotation of the Y268$^{6.51}$ side chain that contributes a significant part of the binding pocket and is roughly parallel to the polyene of the retinal in both structures. Stacking between the phenolic ring of this tyrosine and the retinal polyene is likely important in shaping the slight bend of all-*trans*-retinal towards the covalent bond to K296$^{7.43}$ in TM7. Packing in the two structures further suggest that there is sufficient space for a rotation of retinal inside its mainly hydrophobic binding pocket.

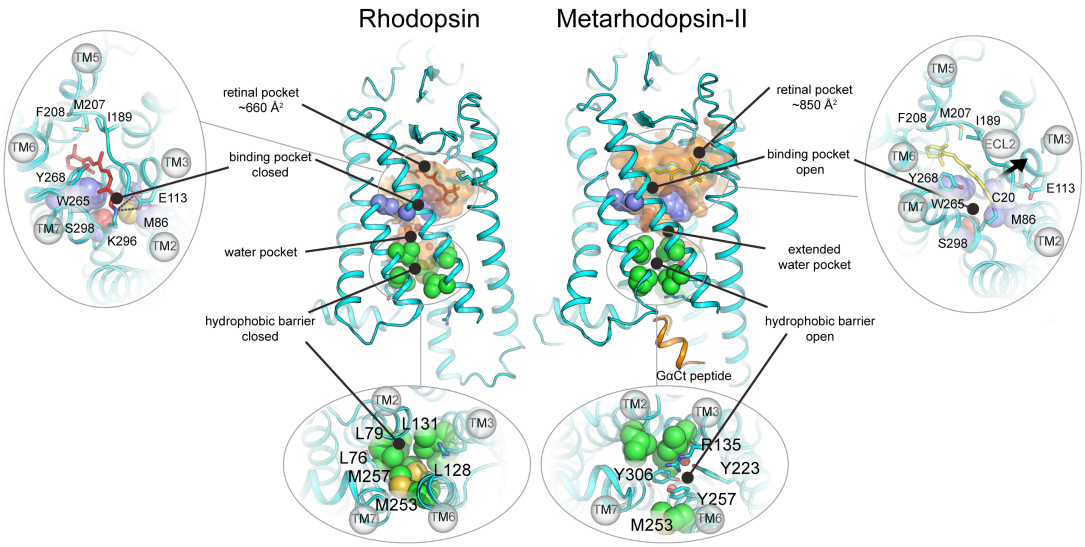

Supplementary Figure 4. Comparison of dark rhodopsin (1GZM, (7)) and metarhodopsin-II obtained from the light activated M257Y$^{6.40}$ mutant. The volume (orange translucent surface) occupied by the ligand (in red for 11-cis and yellow sticks for all-*trans*-retinal, respectively) and the cluster of structural/functional water molecules (red spheres) are highlighted. The top insets show a detail of the binding pocket (viewed from the extracellular side), and highlight the main residues that change conformation as a result of retinal isomerization. Comparing the left and right top panels, it can be seen how M207$^{5.42}$ and F208$^{5.43}$ rearrange, creating space for the β-ionone ring. Also, relocation of C20 in retinal results in a displacement of ECL2 (black arrow). Moreover, the movement of TM2, TM6 and TM7 results in the opening of a gap between residues M86$^{2.53}$, W265$^{6.48}$ and S298$^{7.45}$ (dark blue spheres). The bottom insets show a detail of the cytoplasmic side of the receptors (viewed from the cytoplasm), highlighting how relocation of TM2, TM6 and TM7 also results in the opening of the hydrophobic barrier formed by L76$^{2.43}$, L79$^{2.46}$, L128$^{3.43}$, L131$^{3.46}$, M253$^{6.36}$ and M257$^{6.40}$ (green spheres). Thus, rearrangement of these helices upon activation creates a continuous water pocket extending from the retinal binding site to the ERY motif at the cytoplasmic side that allows relocation of water molecules. In addition, it creates the space for the interaction between the highly conserved residues R135$^{3.50}$, Y223$^{5.58}$ and Y306$^{7.52}$ a key determinant of the active state that is stabilized by the M257Y$^{6.40}$ mutation.

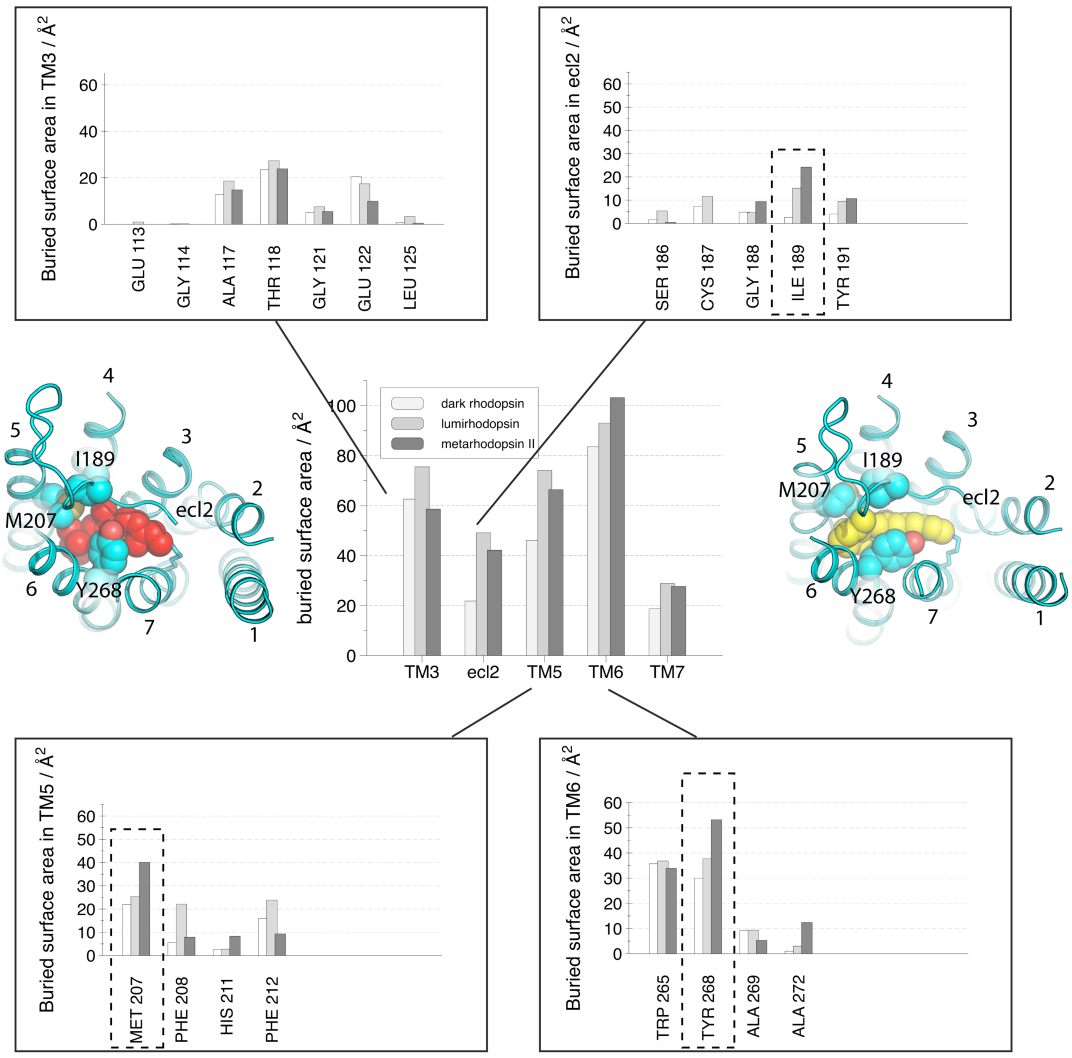

Supplementary Figure 5: Area of rhodopsin (white), lumirhodopsin (grey) and metarhodopsin-II (black) buried by retinal. The central panel shows the total buried surface in TM3, ECL2, TM5, TM6 and TM7, while the insets show the individual contribution of each residue. The graphic shows that the most prominent changes in the contacts between retinal and the protein during activation are due to I189(ECL2), M207(5.42) and Y268(6.51), shown as spheres in the left (rhodopsin) and right (metarhodopsin-II) cartoons. Buried surface areas where calculated with the program PISA(8).

Supplementary Movie. Morph between inactive dark (1GZM (7), red retinal) and the light activated metarhodopsin-II state in the M257$^{Y6.40}$ mutant (4A4M, yellow retinal). Side chains in the retinal binding pocket (E113$^{3.28}$, Y191^{ECL2}, W265$^{6.48}$, P267$^{6.50}$, Y268$^{6.51}$, A272$^{6.55}$, M207$^{5.42}$, F208$^{5.43}$, F212$^{5.47}$, K296$^{7.43}$, S298$^{7.45}$) are shown as sticks. The movie highlights the rearrangement of W265$^{6.48}$ and S298$^{7.45}$ (see Supplementary Figure 4 for details), and of M207$^{5.42}$ and F208$^{5.43}$ (see Supplementary Figures 4 and 5 for details). Also, the movie highlights how retinal rotates around the helix distortion stabilized by P267$^{6.50}$.

Materials and Methods

Protein expression

Bovine rhodopsin containing the stabilizing N2C/D282C and M257Y$^{6.40}$ mutations was cloned into the pACMVtetO vector for tetracycline-inducible expression in mammalian cells(9) using NotI and KpnI restriction sites. The vector was stably transfected into HEK293S-GnTI$^-$ cells with restricted and homogenous N-glycosylation(10).

Cells were expanded as adhesion cultures in DMEM/F12 medium supplemented with FBS (10%), PenStrep (Gibco), Geneticin-G418 (200µg/ml) and blasticidin (5µg/ml). Cells were harvested and further expanded as suspension cultures in a 10l wave bioreactor (GE Healthcare) containing Freestyle Medium (Invitrogen) supplemented with FBS (5%) and PenStrep (Gibco). Once a cell density of 2x10^6 cells/ml was reached, protein expression was induced by addition of 2µg/ml tetracycline and 5mM sodium butyrate. Cells were harvested after 72h and stored at -80°C.

Receptor purification

Cell pellets were solubilized for 1 hour at 4°C with PBS buffer containing protease inhibitor tablets (complete protease inhibitor cocktail tablets, Roche) and 1.25% DM (β-decyl-maltoside). M257Y$^{6.40}$ opsin was bound to 1D4 antibody(11) coupled to CnBr-activated sepharose 4B resin (GE Healthcare) and washed with PBS pH7.0, 0.125% DM. 11-*cis* retinal (50µM) was added and the resin incubated overnight at 4°C to reconstitute ground-state rhodopsin. All steps involving retinal were performed under dim red light. The resin was washed with PBS pH 7.0, 0.125% DM followed by 10mM Hepes pH 7.0, 0.125% DM. The purified protein was eluted in the same buffer supplemented with an elution peptide resembling the C-terminus of rhodopsin (TETSQVAPA, 80µM). For crystallization the buffer was exchanged in a Sephadex200 gel filtration column to 10mM Mes pH 5.0, 100mM NaCl, 1% OG (β-octyl-glycoside).

Purification and spectral analysis of rod opsin

Rod opsins were purified in either their apoprotein form or as a pigment reconstituted with 50 µM all-*trans*-retinal as previously reported(12), except that the final wash steps and elution steps were performed in 10 mM HEPES pH 7.4, 200 M $MgCl_2$, 3 mM NaN_3, 0.02% (w/v) DDM. Spectra were recorded using a Hitachi U-3210 dual-beam spectrophotometer adapted for dark room use by the manufacturer. Acidification of samples for acid-trap experiments was performed by adding 50 mM sodium phosphate buffer, pH 3.5, and 0.5% (w/v) SDS.

G protein activation assay

The G protein transducin was extracted from bovine rod outer segments and purified according to previously published methods(13). Purified G protein was concentrated and dialyzed 3 times against 5 mM Tris (pH 7.4), 1 mM $MgCl_2$, 1 mM DTT, 50% (v/v) glycerol. Following dialysis, purified G protein was stored at -20°C.

G protein activation assays were performed as previously described(14). Pigments for G protein activation assays were formed by incubating 50 nM opsin in 10 mM HEPES pH 7.4, 200 M $MgCl_2$, 3 mM NaN_3, 0.02% (w/v) DDM with 1 μM retinal for 1 hour. Reaction conditions contained 10 mM Tris-Cl pH 7.4, 100 mM NaCl, 5 mM $MgCl_2$, 0.1 mM EDTA, 0.01% DDM (w/v), 1 mM DTT, 3 μM GTPγ^{35}S (specific activity ~1.0 x 10^5 cpm/pmol), 1 μM G protein, and 5 nM purified opsin or pigment. At indicated time points, 10 μl aliquots were collected on a nitrocellulose filter connected to a vacuum manifold. Filters were washed with buffer containing 10 mM Tris-Cl pH 7.4, 100 mM NaCl, 5 mM MgCl2, and 1 mM DTT. Filters were added to scintillation fluid and counts were recorded using a Beckman Coulter LS6500 multi-purpose scintillation counter. Assays were performed with n=3, error bars represent standard error. Activity levels were assessed by fitting the data to a linear regression curve and taking the slope of the curve.

Light activation and crystallization

Reconstituted ground-state rhodopsin was concentrated to 5-7.5 mg/ml (Vivaspin, 50kD cutoff concentrator). The sample was mixed with dried brain lipid extract (Lipid to protein ration of 0.5-1 w/w, Avanti Polar Lipids), briefly sonicated and incubated for 30 minutes in presence of a 10 fold molar excess of peptide resembling the last eleven amino-acids of the Gα subunit of the G protein carrying the mutation K341L (ILENLKDCGLF, Advanced Biomedical). In addition to the 125-200μM 11-*cis*-retinal prebound to the purified receptor, reactions contained 1μM all-*trans*-retinal. Just before crystallization, the receptor was selectively light activated for 5 minutes using a >515nm long pass filter that prevented exposure of free retinal and metarhodopsin-II. The light activated protein was crystallized in the dark by sitting drop vapor diffusion against 3.0-3.4 M ammonium sulphate, 100 mM sodium acetate pH 4.5. Crystals were harvested under dim-red light and soaked in crystallization buffer containing 10% trehalose prior to freezing in liquid nitrogen.

Data collection and structure determination

Data was collected using the micro-focus setup of beamline X06SA at the Swiss Light Source (SLS). Data from 3 crystals were integrated using XDS(15) and brought onto a common scale using SCALA from the CCP4 program suite(16). Phases were obtained by molecular replacement using the program PHASER(17) and the polypeptide of previously crystallized E113Q mutant(4) as search model. The resulting solution was refined using iterative cycles of

model building in COOT(18) and refinement (rigid body, energy minimization, simulated annealing, individual B-factor refinement) with the PHENIX program suite(19). Coordinates and structure factors have been deposited under pdb code 4a4m.

Author contributions. P.C.E. and J.S. performed cloning, initial expression and purification using essential experimental protocols and materials contributed by D.D.O. Receptor activation and retinal binding studies were contributed by B.N. and D.D.O.. P.C.E. created stable cell lines, optimized expression and crystallization and performed crystal cryo-cooling. Initial crystallization was by J.S. who also collected data and refined the structures. Structure analysis and manuscript preparation was done by X.D. and J.S.

References:

1. Alexandrov AI, Mileni M, Chien EY, Hanson MA, & Stevens RC (2008) Microscale fluorescent thermal stability assay for membrane proteins. *Structure* 16(3):351-359.
2. Vogel R & Siebert F (2003) Fourier transform IR spectroscopy study for new insights into molecular properties and activation mechanisms of visual pigment rhodopsin. *Biopolymers* 72(3):133-148.
3. Standfuss J, Zaitseva E, Mahalingam M, & Vogel R (2008) Structural impact of the E113Q counterion mutation on the activation and deactivation pathways of the G protein-coupled receptor rhodopsin. *J Mol Biol* 380(1):145-157.
4. Standfuss J*, et al.* (2011) The structural basis of agonist-induced activation in constitutively active rhodopsin. *Nature* 471(7340):656-660.
5. Nakamichi H & Okada T (2006) Crystallographic analysis of primary visual photochemistry. *Angew Chem Int Ed Engl* 45(26):4270-4273.
6. Nakamichi H & Okada T (2006) Local peptide movement in the photoreaction intermediate of rhodopsin. *Proc Natl Acad Sci U S A* 103(34):12729-12734.
7. Li J, Edwards PC, Burghammer M, Villa C, & Schertler GF (2004) Structure of bovine rhodopsin in a trigonal crystal form. *J Mol Biol* 343(5):1409-1438.
8. Krissinel E & Henrick K (2007) Inference of macromolecular assemblies from crystalline state. *J Mol Biol* 372(3):774-797.
9. Reeves PJ, Kim JM, & Khorana HG (2002) Structure and function in rhodopsin: a tetracycline-inducible system in stable mammalian cell lines for high-level expression of opsin mutants. *Proc Natl Acad Sci U S A* 99(21):13413-13418.
10. Reeves PJ, Callewaert N, Contreras R, & Khorana HG (2002) Structure and function in rhodopsin: high-level expression of rhodopsin with restricted and homogeneous N-glycosylation by a tetracycline-inducible N-acetylglucosaminyltransferase I-negative HEK293S stable mammalian cell line. *Proc Natl Acad Sci U S A* 99(21):13419-13424.
11. Molday RS & MacKenzie D (1983) Monoclonal antibodies to rhodopsin: characterization, cross-reactivity, and application as structural probes. *Biochemistry* 22(3):653-660.
12. Gross AK, Xie G, & Oprian DD (2003) Slow binding of retinal to rhodopsin mutants G90D and T94D. *Biochemistry* 42(7):2002-2008.
13. Wessling-Resnick M & Johnson GL (1987) Allosteric behavior in transducin activation mediated by rhodopsin. Initial rate analysis of guanine nucleotide exchange. *J Biol Chem* 262(8):3697-3705.
14. Zhukovsky EA, Robinson PR, & Oprian DD (1991) Transducin activation by rhodopsin without a covalent bond to the 11-cis-retinal chromophore. *Science* 251(4993):558-560.
15. Kabsch W (1993) Automatic processing of rotation diffraction data from crystals of initially unknown symmetry and cell constants. *J. Appl. Cryst.* 26:795-800.

16. Anonymous (1994) The CCP4 suite: programs for protein crystallography. *Acta Crystallogr D Biol Crystallogr* 50(Pt 5):760-763.
17. McCoy AJ, Grosse-Kunstleve RW, Storoni LC, & Read RJ (2005) Likelihood-enhanced fast translation functions. *Acta Crystallogr D Biol Crystallogr* 61(Pt 4):458-464.
18. Emsley P & Cowtan K (2004) Coot: model-building tools for molecular graphics. *Acta Crystallogr D Biol Crystallogr* 60(Pt 12 Pt 1):2126-2132.
19. Adams PD*, et al.* (2002) PHENIX: building new software for automated crystallographic structure determination. *Acta Crystallogr D Biol Crystallogr* 58(Pt 11):1948-1954.